nature physics

ARTICLES

PUBLISHED ONLINE: 3 JULY 2017 | DOI: 10.1038/NPHYS4180

Contact enhancement of locomotion in spreading cell colonies

Joseph d'Alessandro[1*†], Alexandre P. Solon[2], Yoshinori Hayakawa[3], Christophe Anjard[1], François Detcheverry[1], Jean-Paul Rieu[1] and Charlotte Rivière[1*]

The dispersal of cells from an initially constrained location is a crucial aspect of many physiological phenomena, ranging from morphogenesis to tumour spreading. In such processes, cell–cell interactions may deeply alter the motion of single cells, and in turn the collective dynamics. While contact phenomena like contact inhibition of locomotion are known to come into play at high densities, here we focus on the little explored case of non-cohesive cells at moderate densities. We fully characterize the spreading of micropatterned colonies of *Dictyostelium discoideum* cells from the complete set of individual trajectories. From data analysis and simulation of an elementary model, we demonstrate that contact interactions act to speed up the early population spreading by promoting individual cells to a state of higher persistence, which constitutes an as-yet unreported contact enhancement of locomotion. Our findings also suggest that the current modelling paradigm of memoryless active particles may need to be extended to account for the history-dependent internal state of motile cells.

Understanding how cell assemblies regulate their motility is a major challenge of current biophysics. Indeed, collective effects in the motion of cells play a crucial role *in vivo* in processes such as wound healing[1], tumour progression[2] or morphogenesis[3]. In disentangling the often intricate relationship between the behaviours at the cellular level and the population scale, two basic questions arise: how do cell–cell interactions alter the properties of individual cell motion? How do they impact the population dynamics?

The trajectory of a cell crawling on a surface is akin to a correlated random walk characterized by a persistence time beyond which the motion becomes diffusive[4,5]. In the absence of interactions, this would lead on long time to simple diffusion dynamics at the colony level, as captured in descriptions based on the Fisher–Kolmogorov–Petrovski–Piskunov (FKPP) equation[6,7]. However, the assumption of non-interacting cells is often unwarranted[8,9], as several types of cell–cell interactions affecting the collective dynamics have been uncovered experimentally. A first class involves long-range interactions, which may be mediated by a chemical[10,11] as in quorum sensing, or by the substrate[12]. A second class includes short-range contact interactions: excluded volume (EV), cell–cell adhesion or contact inhibition of locomotion (CIL)[13], which acts to change the direction of motion of a cell upon contact with another cell.

Contact interactions may play an essential role in the collective behaviour of cells. On the edge of a dense colony, CIL[14] or EV[15] combined with a density gradient acts to bias the motion towards free space[9,16,17], hence facilitating the spreading of the colony[8,15,18]. This effect is further reinforced by the tension created by leader cells through adherens junctions[16,19]. In the bulk of a tissue, force transmission through adherens junctions[20,21] (but also nematic alignment[22,23] or simple EV[24]) can lead to coordinated motion over several cell sizes and induce active jamming and glassy behaviour[25–27]. The slowing down of tissue dynamics is especially clear in cell systems dominated by CIL[14], which reduces the cell persistence[28] or effective speed[29]. Whether EV, CIL or adhesion, those interactions are local in nature, and their influence is most pronounced at the highest densities, near close-packing.

Here, we report on a new kind of cell–cell interaction, whose effect persists long after contact and with a global impact on collective spreading, even at moderate densities. We investigate collective migration of cells, lacking both cell adhesion and alignment, in assemblies well below the close-packing. In contrast to the high-density regime, this region has received much less attention so far, despite its unambiguous biological relevance, most notably the spreading of highly metastatic cells[30]. By studying the spreading dynamics of micropatterned *Dictyostelium discoideum* cell colonies, we find that cell–cell contacts enhance the cell persistence, an effect that we refer to as contact enhancement of locomotion (CEL). This phenomenon results in a speed-up of the colony spreading upon increasing the initial packing fraction. It may enable efficient invasion or exploration of the environment, and may be seen as an escape mechanism at the single-cell level. Because the model organism, *Dictyostelium discoideum*, shares many common mechanisms with human leukocytes, amoeboid cancer cells and mammalian cells in general[31], the presence of CEL could potentially impact migration processes and collective dispersal, for example, in inflammatory response or cancer invasion. It also defines a novel kind of interaction, which, in contrast to current framework of active matter based on physical forces, modifies the internal state of the moving agents and their subsequent behaviour.

A highly controlled model of cell colony

We used vegetative *Dictyostelium discoideum* (*D.d.*) cells, a benchmark for the amoeboid motility of fast-moving cells[30,32,33]. They are specially well suited to investigate the role of interactions in the absence of strong cell–cell adhesion, as they do not form such adhesions in nutrient-rich conditions[34]. To experimentally mimic the dispersal of cells from an initial location in a reproducible way,

[1]Université de Lyon, Université Claude Bernard Lyon 1, CNRS, Institut Lumière Matière, F-69622 Villeurbanne, France. [2]Department of Physics, Massachusetts Institute of Technology, Cambridge, Massachusetts 02139, USA. [3]Center for Information Technology in Education, Tohoku University, Sendai 980-8578, Japan. †Present address: Institut Jacques Monod (IJM), CNRS UMR 7592 and Université Paris Diderot, 75013 Paris, France. *e-mail: joseph.dalessandro@wanadoo.fr; charlotte.riviere@univ-lyon1.fr

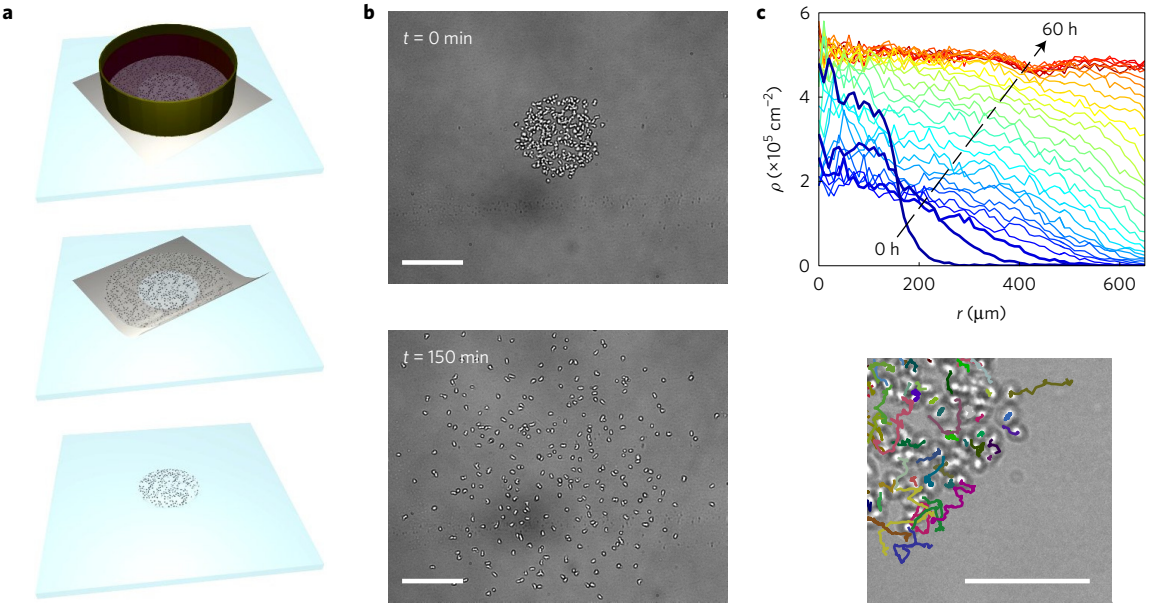

Figure 1 | A highly controlled experimental set-up gives full access to colony spreading dynamics at both individual and population scales. a, Cartoon of the patterning technique. The cells are first deposited in a home-made well (brown) on top of a PDMS stencil (light grey) made by soft-lithography techniques (top). After 45 min of adhesion, the well and the stencil are removed (centre), creating an initial circular pattern of 320 μm in diameter (bottom), whose spreading is then followed by time-lapse microscopy. **b**, Snapshots of a colony with $N_0 = 245$ cells initially at $t = 0$ min (top) and $t = 150$ min (bottom). Scale bars, 200 μm. **c**, Top: evolution of the density profiles $\rho(r,t)$ over 60 h (from blue to red) for one colony with initially $N_0 = 349$ cells. All the curves are separated by a 2 h interval. The first three curves are drawn thicker to highlight the fast initial spreading of the colony. Bottom: cell trajectories at the edge of the initial spot, from $t = 0$ min to $t = 60$ min. Scale bar, 100 μm.

we constrained a controlled number of cells in a disk of diameter 320 μm, using polydimethylsulfoxide (PDMS) micro-stencils[16,35] (Fig. 1a). Taking off the micro-stencil, we let them migrate freely outwards and image the colony for durations ranging from 8 h to 48 h (see snapshots in Fig. 1b and Supplementary Movie 1).

We characterize the colony spreading both at the population and individual cell levels (Fig. 1c). Making use of the circular symmetry, field quantities such as the density (Fig. 1c) are averaged over concentric rings and depend only on time t and the distance r from the centre of the colony. At short times, we first observe a decrease of the density in the centre of the colony as it spreads to invade free space. Then, on timescales of the order of the doubling time $\beta^{-1} \sim 9$ h, the density starts increasing uniformly because of cell divisions. Finally, after about 40 h the density saturates at a carrying capacity $\rho_{\max} \approx 5\text{–}8 \times 10^5$ cell cm^{-2} (Fig. 1c).

At long times, the spreading of the colony is dominated by interactions through soluble molecules. Using the single-cell trajectories obtained by automated cell tracking, we observe that, after an initial increase, the average cell speed (see Supplementary Fig. 1) decreases until it reaches a low-motility plateau at $t \approx 10$ h. This behaviour at long times is well explained by the overall regulation of the motility through a secreted quorum-sensing factor, which has been evidenced in our group before[10]. Indeed, when repeating the spreading experiments with a continuous perfusion of fresh medium to rinse out secreted molecules, the decrease in motility is suppressed and the colony instead rapidly reaches a high-motility plateau (see Supplementary Fig. 1a). As soon as the perfusion stops, the concentration of quorum-sensing factors builds up and the cell speed drops. We now focus on the short-time spreading of the colony.

Collective effects on the short-time spreading

A series of experiments at various colony densities brings the first key observation of this work: the higher the cell density, the faster the colony spreads (Fig. 2a,b and Supplementary Movies 2 and 3). This collective effect is seen both on the density profiles or on the gyration radius, $R_g = \sqrt{\langle r^2 \rangle}$, which quantifies the size of the colony (see Fig. 2c–e). It is also visible at the individual cell level. Computing the radial velocity v_r of each cell, and taking an average over the whole colony, we find that $\langle v_r \rangle$ exhibits a positive peak around $t = 100$ min in the colonies with higher initial cell number $N_0 = 246 \pm 66$ (Fig. 2f). The existence of a non-vanishing radial velocity is not surprising in itself since it is the analogue, for self-propelled particles[36], of an outward diffusive flux. However, one expects the peak to be located at a time of the order of the persistence time of the particles, which is found around a few minutes for *D.d.* cells in similar conditions[10,37]. In contrast, the radial velocity peak happens here on a much longer timescale (∼100 min).

The amplitude of the peak in radial velocity strongly increases with the number of cells in the colony (Fig. 2f), indicating that an unknown effect speeds up the spreading at intermediate timescales. Importantly, this effect neither originates from cell division (it happens on a timescale much shorter than the doubling time) nor from distant chemically mediated interactions arising from secreted or depleted soluble molecules (see Supplementary Fig. 1) or from deposited trails (see Supplementary Fig. 2). This suggests that the primary cause for this density-dependent spreading dynamics involves local interactions, here understood as collisions or short-range interactions, (that is, occurring when cells are in contact or in close vicinity). To ascertain this point, we now turn to a more refined analysis of the motion of individual cells.

Cell–cell contacts increase the persistence

From our dataset of trajectories, we compare cell motion at the lowest and highest initial densities, with $\langle N_0 \rangle = 35$ and $\langle N_0 \rangle = 246$, respectively (Fig. 3a–d). A striking difference immediately appears when examining an array of trajectories (Fig. 3b and Supplementary Fig. 4): the persistence is higher in the denser colony. This observation is corroborated by looking at the coefficient of movement efficiency (CME, see Methods), which allows one to estimate the persistence of the trajectories with good time and space accuracy. For a given interrogation time Δt, the quantity CME(Δt) ranges from 0 for a motion with persistence time much smaller than

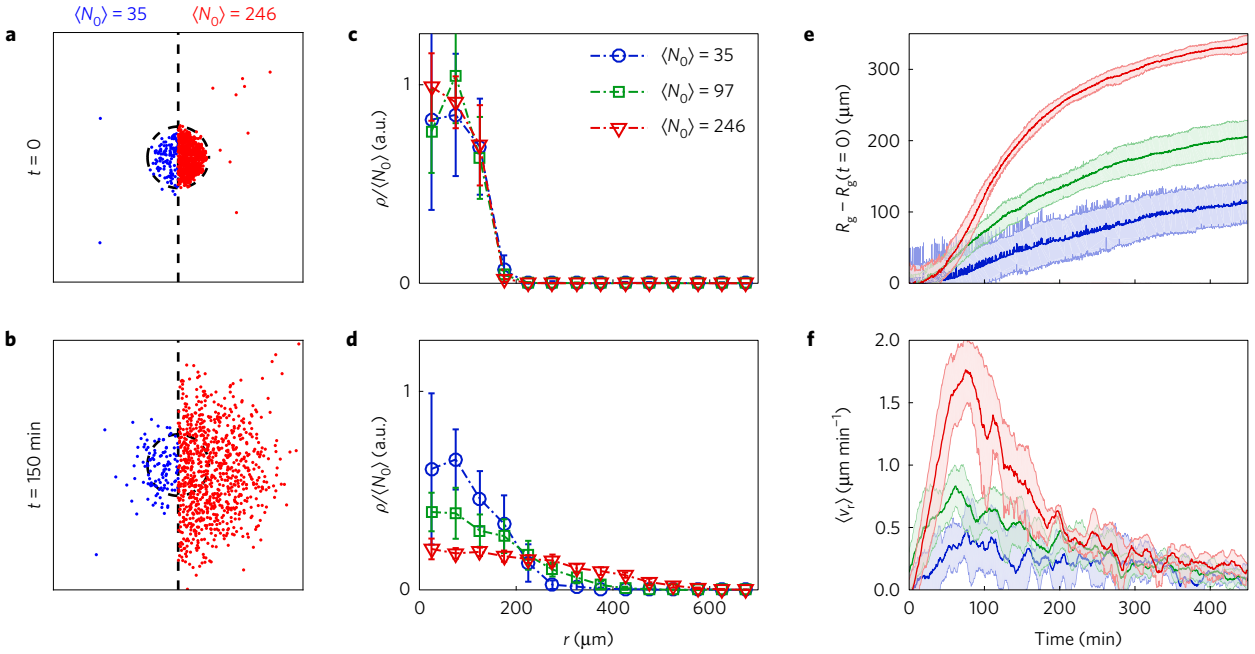

Figure 2 | Density-dependent colony spreading. The experiments are divided into three groups to study the effect of the initial cell number N_0. **a**,**b**, Juxtaposed 'snapshots' of the colonies for two different groups $N_0 = 35 \pm 12$ (blue, left, 208 cells in total) and 246 ± 66 (red, right, 1,229 cells in total), at $t = 0$ and $t = 150$ min. The positions of all cells in each group of experiments are represented as coloured points. The dashed circle denotes the edge of the stencil. **c**,**d**, Normalized density profiles for each group at $t = 0$ min (**c**) and $t = 150$ min (**d**). **e**, Gyration radius $R_g = \sqrt{\langle r^2 \rangle}$ of the colonies as a function of time. **f**, Radial velocity $\langle v_r \rangle$ as a function of time averaged over the colony (same colour code for every panel). The error bars (**c**,**d**) and shaded areas (**e**,**f**) represent the standard deviation ($n = 6, 8, 5$ experiments, respectively, for $N_0 = 35 \pm 12$, $N_0 = 97 \pm 25$, $N_0 = 246 \pm 66$).

Δt to 1 for ballistic motion. From the spatio-temporal evolution of the CME measured with $\Delta t = 5$ min, it is clear that the persistence increases with density (Fig. 3c). The trend is especially pronounced at short times and near the periphery of the colony, where the radial velocity map also exhibits high values (Fig. 3d). A further hint of change in persistence is provided by the cell shape: the cells appear more elongated, hence more polarized, in denser colonies. While already visible qualitatively in Fig. 3a, it is confirmed quantitatively by computing the cell contours' eccentricity, which increases with density at early times before relaxing to values corresponding to more isotropic cell shapes (see Supplementary Fig. 3).

Summarizing our observations so far, we see that denser colonies spread faster, because cell motion is more persistent, an effect probably due to local interactions (contacts). We are thus led to the rather counter-intuitive hypothesis that contacts may enhance persistence. To assess its validity, we compare the statistics of individual cell motion before and after a contact. As described in the Supplementary Information, we retain only 'clean' contacts between cells undergoing no other collision in a ± 15 min time span. We consider the velocity v and CME, each normalized by their basal values $\bar{v}$ and $\overline{\mathrm{CME}}$ (Fig. 3e,f and Supplementary Figs 10 and 11). The two quantities, which involve an average over several hundreds of contact events, exhibit a sharp increase amounting to 30% and 10%, respectively, followed by a slower decay with typical time on the order of 10 min. This is the second key observation: the phenomenon of a cell increasing its persistence after contact with another cell. Paralleling the definition of CIL[13], hereafter we refer to this effect as CEL. Note that in self-propelled rods and elongated bacteria, contacts may enhance the persistence by reducing the angular noise[38,39]. However, CEL is clearly distinct from this mechanism because it acts not only during contact, but persists long afterwards. In addition, the analysis of 'scattering angles' in collision events (see Supplementary Figs 8 and 9) show that cell–cell contacts have no aligning effect likely to promote collective motion and to increase the spreading rate by itself.

A minimal model

We now introduce a primitive model of CEL, based on the premise that a contact transiently enhances persistence. Specifically, a cell may exist in two states: a mode 1 (basal) and a mode 2 (activated) of higher persistence. They differ only by their persistence times ${D_{r2}}^{-1} > {D_{r1}}^{-1}$, D_{ri} being the rotational diffusion coefficient of direction vector in mode i. Upon a single contact, cells in mode 1 instantaneously switch to mode 2, where they remain for an exponentially distributed time with mean τ_2, before reverting back to the basal state. Many refinements would be possible to these basic picture, including finite-time transition or gradual increment in persistence through accumulation of contacts. Note that the velocity modulus is the same in both mode. While this may appear contrary to Fig. 3e, we note that our experimental v is not a pure velocity magnitude, but is influenced by the persistence time. Besides, the choice of changing only the persistence time allows one to reduce the number of parameters in the model. Although admittedly oversimplified, our description will prove sufficient to capture the main experimental feature, both at the cell and population levels.

Modelling individual cell motion

We first focus on the individual trajectories, and assuming for simplicity that time spent in mode 1 is again exponentially distributed, introduce its mean τ_1. Though τ_1 slowly evolves with time in a density-dependent manner due to changes in the collision frequency, we take it as constant (see Supplementary Information for a discussion of this hypothesis). Those assumptions completely define a bimodal pattern of motion, which can be entirely characterized analytically (see Supplementary Information). The velocity direction autocorrelation function turns out to be the sum of two exponentials

$$C(t) \equiv \langle \mathbf{u}(t_o) \cdot \mathbf{u}(t_o + t) \rangle_{t_o} = c\, \mathrm{e}^{-\gamma t} + c'\, \mathrm{e}^{-\gamma' t} \qquad (1)$$

where $\mathbf{u}$ is the direction vector of cell motion and c, c', γ and γ' are explicitly known as functions of τ_1, τ_2, D_{r1} and D_{r2}. Qualitatively,

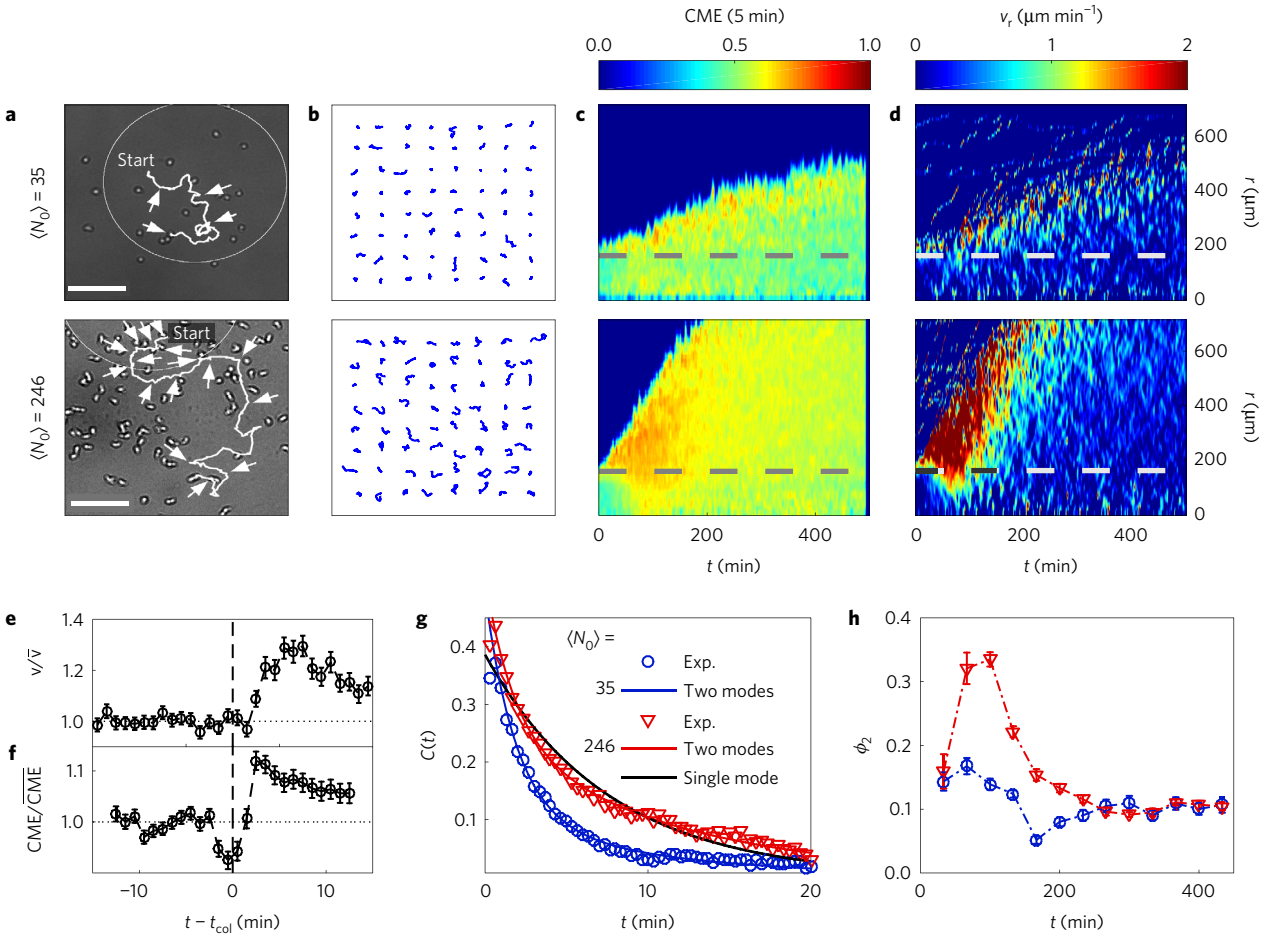

Figure 3 | Local interactions between cells lead to an increase in cell persistence. a–d, Comparison of trajectory properties at low ($\langle N_0 \rangle = 35$, top row) and high ($\langle N_0 \rangle = 246$, bottom row) initial densities. **a**, Typical cell trajectory (plotted over 100 min), with the white circle representing the border of the initial pattern and the arrows pointing to collision events. **b**, 64 randomly picked trajectories from $t = 100$ min to $t = 130$ min. **c**,**d**, Spatio-temporal dynamics of the CME with $\Delta t = 5$ min (**c**) and of the radial velocity v_r (**d**) (the dashed lines represent the border of the initial colonies). **e**,**f**, Normalized speed (**e**) and CME (**f**) computed with $\Delta t = 5$ min for cells undergoing a single collision at $t = t_{col}$ within a 30-min-long interval. $\bar{v}$ (resp. $\overline{CME}$), denote the basal speed (resp. CME) before collision. The error bars show the SEM for the $n = 464$ segments of trajectory from 232 collisions. **g**, Velocity direction autocorrelation function at $t = 67 - 133$ min for $\langle N_0 \rangle = 35$ and 246 (symbols) and fits using equation (1) (solid lines) with $D_{r1}^{-1} = 2$ min and $\tau_2 = 10$ min. The thick black line represents the best single-exponential ('Single mode') fit for $\langle N_0 \rangle = 246$, which misses the experimental behaviour at both very short and long times. **h**, Proportion ϕ_2 of cells in mode 2 extracted from the fit of the correlation functions as explained in the Supplementary Information (the lines are guides for the eye, same colours and symbols as in **g**). The error bars represent the 95% confidence interval for the fit parameter estimation.

we have observed that when fitting our experimental data, this form provides a much better fit than the monoexponential decay that arises in the simplest models (Ornstein–Uhlenbeck, active Brownian particle or run-and-tumble), as illustrated in Fig. 3g. Quantitatively, we used equation (1) to fit all experimental velocity correlation functions, as detailed in the Supplementary Information. To reduce the number of free parameters, motion in mode 2 is taken as ballistic ($D_{r2} = 0$). As an output, we obtain two parameters common to all curves: $D_{r1}^{-1} = 2$ min and the mean time in mode 2, $\tau_2 = 10$ min, whose order of magnitude is completely consistent with the decay observed in Fig. 3e–f. Besides, we get the (time-dependent) mean time in mode 1 $\tau_1(t)$, from which we deduce the fraction $\phi_2(t) = \tau_2/(\tau_1 + \tau_2)$ of cells in mode 2 (Fig. 3h). While ϕ_2 remains near 10% at $\langle N_0 \rangle = 35$ at all times, it is three times higher in the early stage for $\langle N_0 \rangle = 246$, a significant increase that can be rationalized with simple estimates of the mean collision time[58] (see Supplementary Information). Overall, our elementary CEL model allows an understanding of the biexponential relaxation of velocity, and supports the idea that higher densities indeed promote switching to the persistent mode.

Modelling collective spreading dynamics

We now turn to the consequences of our minimal CEL model on the spreading dynamics, and show that in contrast to alternative models of simple contact interactions, it is sufficient to account for all salient features. Our starting point is the active Brownian particle (ABP) model, well-studied as a minimal model of active particles[29,40], and a suitable basis for modelling the persistent random motion of cells. Self-propelled hard disks move at a constant velocity v, and their direction of motion θ is subject to rotational diffusion with coefficient D_r. The equations of motion for the ith particle are

$$\partial_t \mathbf{r}_i = v\mathbf{u}(\theta_i) + \sum_{j \neq i} \mathbf{f}_{ij}(\mathbf{r}_i - \mathbf{r}_j), \quad \partial_t \theta_i = \sqrt{2D_r}\eta_i(t) \qquad (2)$$

where $\mathbf{u}(\theta_i) = (\cos\theta_i, \sin\theta_i)$, η_i is a delta-correlated Gaussian white noise with zero mean and unit variance and $\mathbf{f}_{ij}$ is the steric repelling force exerted by particle j on particle i (see Methods), that accounts for excluded volume. Consistently with the experiments, we take $v = 5\,\mu$m min^{-1}, set $D_r^{-1} = 5$ min to match the average persistence time of experimental trajectories, and initially place the particles in a disk of 320 μm in diameter. The resulting average radial velocity

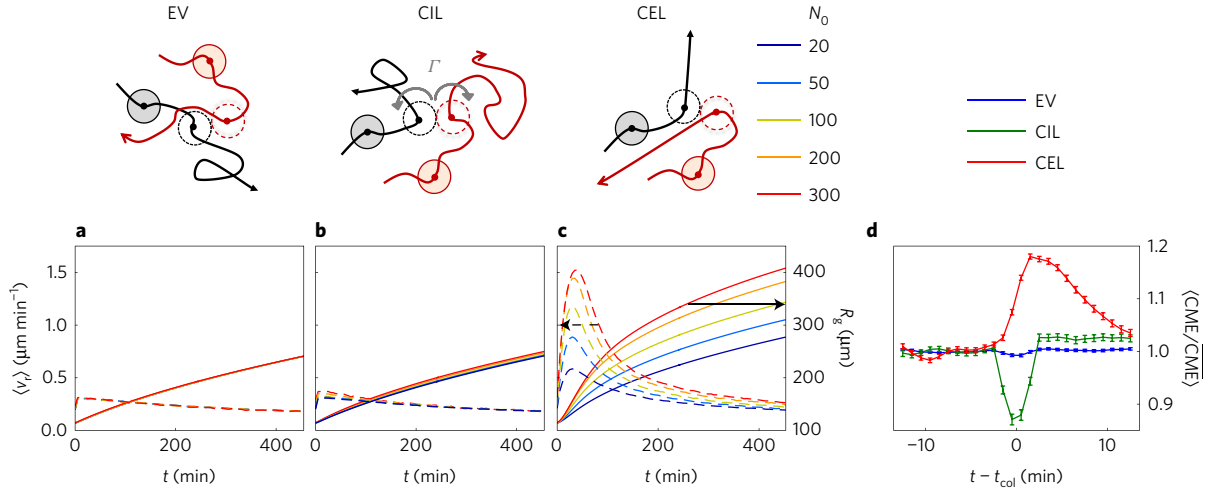

Figure 4 | Spreading colonies in individual-based models with various interaction rules. a–c, Radial velocity $\langle v_r \rangle$ (dashed lines, left axes) and colony radius R_g (solid lines, right axes) in simulated colonies with different numbers of particles N_0 with the three interaction rules considered. The cartoons illustrate the different contact rules: EV only (**a**), EV and CIL (**b**), EV and CEL (**c**). **d**, Single-cell-normalized CME around collisions with various interaction rules. Mean ± s.e.m., $t_{free} = 15$ min.

and radius of gyration measured in the simulations are shown as a function of time in Fig. 4.

Let us first consider the effect of excluded volume alone. Intuitively, one might anticipate a density-dependent spreading induced by an outward pressure[40], an effect demonstrated in Brownian hard spheres, where the effective diffusion coefficient increases with concentration[41]. However, in the present experiments where cells are relatively sparse—with packing fractions up to 0.3—this pressure is not expected to play an important role and, indeed, simulations confirm that the effect of density is negligible (Fig. 4a). Next, we consider the effect of CIL: upon collision, cells reorient away from the contact. To that end, we added an angular repulsion to the equations of motion (keeping EV), in the form of a torque acting on cells undergoing a contact (see Methods), and which acts on typical time Γ^{-1}. Qualitatively, one could imagine that by reorienting the direction of motion of particles towards free space, active reorientation could explain the experimental data[14]. However, even with a large value $\Gamma = 100\ \mathrm{min}^{-1}$ corresponding to quasi-instantaneous reorientation, the density-dependent increase in average radial velocity and spreading rate is an order of magnitude smaller than in the experiment (Fig. 4b). In addition, the (very limited) peak in radial velocity appears at a very early time, at odds with the experimental observation.

Finally, we tested our minimal model of CEL. We fix ${D_{r1}}^{-1} = 2$ min and $\tau_2 = 10$ min, as found above from our analysis of the experimental velocity correlation functions, (mode 2 is again assumed ballistic, with ${D_{r2}}^{-1} = 0$). Note that τ_1 is not a parameter here. Instead switching to mode 2 is governed by collisions that are monitored throughout the simulation, and whose rate depends on local density and time. We find that in contrast to EV alone and CIL, the CEL model captures well the collective spreading of the colony. Indeed, as shown in Fig. 4c, the amplitude and density dependence of the peak in radial velocity, as well as the faster increase of R_g at higher density, are well described. Given the simplicity of the model, the agreement between simulations and experiments appears surprisingly good (see Supplementary Movies 2–5 for a visual comparison).

As a final test, we come back to the statistics of persistence before and after contacts, and analyse simulation data as done above for experiments (Fig. 4d). In the EV case, no significant effect is seen. Adding CIL yields a pronounced minimum, approximately symmetric around the collision time. In contrast, in the CEL model, post-contact persistence exhibits a rapid increase followed by relaxation, in qualitative agreement with experiments. Taken together, our modelling results strongly suggest that CEL is the key ingredient at play here.

Discussion

By investigating the spreading of a colony, we showed that cell contacts enhance the persistence of the cell motion, implying a bimodal behaviour of cells and resulting in a density-dependent dispersal. The latter is reminiscent of swarming colonies of myxobacteria, whose rate of expansion increases with the initial density[42]. Such phenomenon, originally ascribed to 'motility-enhancing interaction'[43], is now thought to involve the deposition of exopolysaccharides that enable motility of cells[44]. Because swarms are very different from our system—they form multi-layered, branching patterns of millions of high-aspect ratio individuals–, the parallel is only phenomenological, the mechanisms at play at the cell level being completely different. As regards the bimodal behaviour involved, there has been growing evidence in the past few years that the persistence may be modulated in random cell migration[45–49]. Our findings add a new piece to this picture. Whereas the mechanism triggering persistence modulation often remains unknown, in this work it is clearly identified as cell–cell contacts.

If this CEL effect is here demonstrated on *D.d.* cells, we expect it to be relevant in a much wider context. Indeed *D.d.* shares many common mechanisms with human leukocytes[32] or amoeboid cancer cells[31]. Like CIL, which has been shown to play a major role in a variety of situations and cell types[14], the presence of CEL could potentially impact different physiological phenomena. Because motion is hampered by EV effects at highest densities near close-packing and contacts will be rare at the lowest densities, we expect that the effect of CEL will be most visible in colonies of intermediate density. Even for very dense colonies, its influence may always be seen near the boundary: just as CIL reorientation may bias motion outwards[3,50], CEL may induce cell to evade in free space after a few contacts. The two processes could also act simultaneously, reinforcing each other's consequences.

On general grounds, CEL behaviour is expected to foster efficient invasion or exploration of surrounding environment, a feature that may be paramount for immune or highly metastatic cells, as well as in morphogenesis and microbial dispersal. Interestingly, it should be noticed that CEL provides at the single-cell level a mechanism reminiscent of escape behaviours, found in a variety of higher

organisms, which involve a temporary change of the displacement pattern and can lead to rich collective effects[51].

Looking forward, two related questions emerge for future work. First, CEL here is triggered by contact between two identical cells; would it also occur for contacts between heterotypic cells or with a wall? Second, what are the cellular processes involved in CEL? Although first observed more than half a century ago, and in spite of recent progress[14,52], the mechanism of CIL is not yet fully elucidated. We can only speculate on that responsible for CEL, but we suspect that CIL and CEL mechanisms may not be mutually exclusive and could even share a common microscopic origin. Indeed, the current explanation for CIL is that the protrusions driving the motion are inhibited in the contact region[14]. Other protrusions can thus develop elsewhere on the cell's periphery, leading to a new direction of motion. We could hypothesize that, similarly, either the inhibition of ruffling in the contact region or the stabilization of the new protrusions reinforces the new polarity, thereby increasing the speed and persistence of the motion. Interestingly, those two possibly concurrent outcomes of cell–cell contacts—immediate CIL and long-lasting CEL—would illustrate the high plasticity of *Dictyostelium*'s cytoskeleton dynamics: while, in response to chemical or mechanical stimuli, the acto-myosin can reorganize in tens of seconds[53,54]—a timescale comparable to the contact duration—it can also remain stably polarized for several minutes afterwards[54]. Only with a detailed understanding of intracellular mechanism can we predict when CEL will be at work and dominate the cell collective dynamics.

On a different note, we finally point out that CEL pertains to a class of models different than the current framework of active matter. The latter is based on self-propelled particles, interacting instantaneously through physical forces that are often both local in time and space, such as the EV and CIL considered above[50,55–57]. In contrast, the CEL model relies on agents endowed with internal states and memory. As a result, the effect of a contact (interaction) may still persist long after it took place, and far from it. This situation might be widespread with biological cells and call for a paradigm different from the physicist's particles.

Methods

Methods, including statements of data availability and any associated accession codes and references, are available in the online version of this paper.

Received 12 May 2016; accepted 22 May 2017; published online 3 July 2017

References

1. Friedl, P. & Gilmour, D. Collective cell migration in morphogenesis, regeneration and cancer. *Nat. Rev. Mol. Cell Biol.* **10,** 445–457 (2009).
2. Friedl, P. & Wolf, K. Tumour-cell invasion and migration: diversity and escape mechanisms. *Nat. Rev. Cancer* **3,** 362–374 (2003).
3. Carmona-Fontaine, C. *et al*. Contact inhibition of locomotion *in vivo* controls neural crest directional migration. *Nature* **456,** 957–961 (2008).
4. Selmeczi, D. *et al*. Cell motility as random motion: a review. *Eur. Phys. J. Spec. Top.* **157,** 1–15 (2008).
5. Li, L., Norrelkke, S. F. & Cox, E. C. Persistent cell motion in the absence of external signals: a search strategy for eukaryotic cells. *PLoS ONE* **3,** e2093 (2008).
6. Kolmogorov, A., Petrovskii, I. & Piscounov, N. A study of the diffusion equation with increase in the amount of substance, and its application to a biological problem. *Math. Mech.* **1,** 1–25 (1937).
7. Simpson, M. J. *et al*. Quantifying the roles of cell motility and cell proliferation in a circular barrier assay. *J. R. Soc. Interface* **10,** 20130007 (2013).
8. Sengers, B. G., Please, C. P. & Oreffo, R. O. C. Experimental characterization and computational modelling of two-dimensional cell spreading for skeletal regeneration. *J. R. Soc. Interface* **4,** 1107–1117 (2007).
9. Marel, A. K. *et al*. Flow and diffusion in channel-guided cell migration. *Biophys. J.* **107,** 1054–1064 (2014).
10. Golé, L., Rivière, C., Hayakawa, Y. & Rieu, J. P. A quorum-sensing factor in vegetative *Dictyostelium discoideum* cells revealed by quantitative migration analysis. *PLoS ONE* **6,** 1–9 (2011).
11. Phillips, J. & Gomer, R. A secreted protein is an endogenous chemorepellant in *Dictyostelium discoideum*. *Proc. Natl Acad. Sci. USA* **109,** 10990–10995 (2012).
12. Angelini, T. E., Hannezo, E., Trepat, X., Fredberg, J. J. & Weitz, D. A. Cell migration driven by cooperative substrate deformation patterns. *Phys. Rev. Lett.* **104,** 168104 (2010).
13. Abercrombie, M. & Heaysman, J. E. Observations on the social behaviour of cells in tissue culture: I. Speed of movement of chick heart fibroblasts in relation to their mutual contacts. *Exp. Cell Res.* **5,** 111–131 (1953).
14. Stramer, B. A. & Mayor, R. Mechanisms and *in vivo* functions of contact inhibition of locomotion. *Nat. Rev. Mol. Cell Biol.* **118,** 43–55 (2016).
15. Dyson, L. & Baker, R. E. The importance of volume exclusion in modelling cellular migration. *J. Math. Biol.* **71,** 679–711 (2014).
16. Serra-Picamal, X. *et al*. Mechanical waves during tissue expansion. *Nat. Phys.* **8,** 628–634 (2012).
17. Nnetu, K. D., Knorr, M., Strehe, D., Zink, M. & Käs, J. A. Directed persistent motion maintains sheet integrity during multi-cellular spreading and migration. *Soft Matter* **8,** 6913–6921 (2012).
18. Yates, C. A., Parker, A. & Baker, R. E. Incorporating pushing in exclusion-process models of cell migration. *Phys. Rev. E* **91,** 052711 (2015).
19. Sepúlveda, N. *et al*. Collective cell motion in an epithelial sheet can be quantitatively described by a stochastic interacting particle model. *PLoS Comput. Biol.* **9,** e1002944 (2013).
20. Petitjean, L. *et al*. Velocity fields in a collectively migrating epithelium. *Biophys. J.* **98,** 1790–1800 (2010).
21. Tambe, D. T. *et al*. Collective cell guidance by cooperative intercellular forces. *Nat. Mat.* **10,** 469–475 (2011).
22. Coburn, L., Cerone, L., Torney, C., Couzin, I. D. & Neufeld, Z. Interactions lead to coherent motion and enhanced chemotaxis of migrating Cells. *Phys. Biol.* **10,** 046002 (2013).
23. Duclos, G., Garcia, S., Yevick, H. G. & Silberzan, P. Perfect nematic order in confined monolayers of spindle-shaped cells. *Soft Matter* **10,** 2346–2353 (2014).
24. Londono, C. *et al*. Nonautonomous contact guidance signaling during collective cell migration. *Proc. Natl Acad. Sci. USA* **111,** 1807–1812 (2014).
25. Angelini, T. E. *et al*. Glass-like dynamics of collective cell migration. *Proc. Natl Acad. Sci. USA* **108,** 4714–4719 (2011).
26. Park, J.-A. *et al*. Unjamming and cell shape in the asthmatic airway epithelium. *Nat. Mat.* **14,** 1040–1049 (2015).
27. Garcia, S. *et al*. Physics of active jamming during collective cellular motion in a monolayer. *Proc. Natl Acad. Sci. USA* **112,** 15314–15319 (2015).
28. Vedel, S., Tay, S., Johnston, D. M., Bruus, H. & Quake, S. R. Migration of cells in a social context. *Proc. Natl Acad. Sci. USA* **110,** 129–134 (2013).
29. Fily, Y. & Marchetti, M. C. Athermal phase separation of self-propelled particles with no alignment. *Phys. Rev. Lett.* **108,** 235702 (2012).
30. Friedl, P. & Wolf, K. Plasticity of cell migration: a multiscale tuning model. *J. Cell Biol.* **188,** 11–19 (2010).
31. Artemenko, Y., Lampert, T. J. & Devreotes, P. N. Moving towards a paradigm: common mechanisms of chemotactic signaling in *Dictyostelium* and mammalian leukocytes. *Cell. Mol. Life Sci.* **71,** 3711–3747 (2014).
32. Friedl, P., Borgmann, S. & Bröcker, E. B. Amoeboid leukocyte crawling through extracellular matrix: lessons from the *Dictyostelium* paradigm of cell movement. *J. Leukoc. Biol.* **70,** 491–509 (2001).
33. Levine, H. Learning physics of living systems from *Dictyostelium*. *Phys. Biol.* **11,** 053011 (2014).
34. Coates, J. C. & Harwood, A. J. Cell–cell adhesion and signal transduction during *Dictyostelium* development. *J. Cell Sci.* **114,** 4349–4358 (2001).
35. Poujade, M. *et al*. Collective migration of an epithelial monolayer in response to a model wound. *Proc. Natl Acad. Sci. USA* **104,** 15988–15993 (2007).
36. Cates, M. E. & Tailleur, J. When are active Brownian particles and run-and-tumble particles equivalent? consequences for motility-induced phase separation. *Europhys. Lett.* **101,** 20010 (2013).
37. Bosgraaf, L. & Van Haastert, P. J. M. The ordered extension of pseudopodia by amoeboid cells in the absence of external cues. *PLoS ONE* **4,** e5253 (2009).
38. Peruani, F., Deutsch, A. & Bär, A. Nonequilibrium clustering of self-propelled rods. *Phys. Rev. E* **74,** 030904 (2006).
39. Peruani, F. *et al*. Collective motion and nonequilibrium cluster formation in colonies of gliding bacteria. *Phys. Rev. Lett.* **108,** 098102 (2012).
40. Solon, A. P. *et al*. Pressure and phase equilibria in interacting active Brownian spheres. *Phys. Rev. Lett.* **114,** 198301 (2015).
41. Bruna, M. & Chapman, S. J. Excluded-volume effects in the diffusion of hard spheres. *Phys. Rev. E* **85,** 011103 (2012).
42. Kaiser, D. Bacterial swarming: a re-examination of cell-movement patterns. *Curr. Biol.* **17,** R561–R570 (2007).
43. Kaiser, D. & Crosby, C. Cell movement and its coordination in swarms of *Myxococcus xanthus*. *Cell Motil.* **3,** 227–245 (1983).

44. Patra, P., Kissoon, K., Cornejo, I., Kaplan, H. B. & Igoshin, O. A. Colony expansion of socially motile *Myxococcus xanthus* cells is driven by growth, motility, and exopolysaccharide production. *PLoS Comput. Biol.* **12,** e1005010 (2016).
45. Potdar, A. A., Jeon, J., Weaver, A. M., Quaranta, V. & Cummings, P. T. Human mammary epithelial cells exhibit a bimodal correlated random walk pattern. *PLoS ONE* **5,** e9636 (2010).
46. Li, L., Cox, E. C. & Flyvbjerg, H. 'Dicty dynamics': *Dictyostelium* motility as persistent random motion. *Phys. Biol.* **8,** 046006 (2011).
47. Bénichou, O., Loverdo, C., Moreau, M. & Voituriez, R. Intermittent search strategies. *Rev. Mod. Phys.* **83,** 81–129 (2011).
48. Metzner, C. *et al*. Superstatistical analysis and modelling of heterogeneous random walks. *Nat. Commun.* **6,** 7516 (2015).
49. Lavi, I., Piel, M., Lennon-Duménil, A.-M., Voituriez, R. & Gov, N. S. Deterministic patterns in cell motility. *Nat. Phys.* **12,** 1146–1152 (2016).
50. Zimmermann, J., Camley, B. A., Rappel, W.-J. & Levine, H. Contact inhibition of locomotion determines cell–cell and cell-substrate forces in tissues. *Proc. Natl Acad. Sci. USA* **113,** 2660–2665 (2016).
51. Ramdya, P. *et al*. Mechanosensory interactions drive collective behaviour in *Drosophila*. *Nature* **519,** 233–236 (2015).
52. Roycroft, A. & Mayor, R. Molecular basis of contact inhibition of locomotion. *Cell. Mol. Life Sci.* **73,** 1119–1130 (2016).
53. Etzrodt, M. *et al*. Time-resolved responses to chemoattractant, characteristic of the front and tail of *Dictyostelium* cells. *FEBS Lett.* **580,** 6707–6713 (2006).
54. Dalous, J. *et al*. Reversal of cell polarity and actin-myosin cytoskeleton reorganization under mechanical and chemical stimulation. *Biophys. J.* **94,** 1063–1074 (2008).
55. Davis, J. R. *et al*. Emergence of embryonic pattern through contact inhibition of locomotion. *Development* **139,** 4555–4560 (2012).
56. Camley, B. A., Zimmermann, J., Levine, H. & Rappell, W.-J. Emergent collective chemotaxis without single-cell gradient sensing. *Phys. Rev. Lett.* **116,** 098101 (2016).
57. Szabo, A. *et al*. *In vivo* confinement promotes collective migration of neural crest cells. *J. Cell. Biol.* **213,** 543–555 (2016).
58. Berezhkovskii, A. M., Makhnovskii, Y. A. & Suris, R. A. Wiener sausage volume moments. *J. Stat. Phys.* **57,** 333–346 (1989).

Acknowledgements

The authors are grateful to R. Fulcrand for his help in micro-fabrication, to V. Hakim for stimulating discussions and to C. Cottin-Bizonne for her comments on the manuscript. J.d'A. has been partially supported by the Fondation ARC pour la Recherche sur le Cancer and by the Programme d'Avenir Lyon-Saint Étienne. A.S. acknowledges funding through a PLS fellowship of the Gordon and Betty Moor foundation. J.d'A., C.R. and J.-P.R. belong to the CNRS consortium CellTiss and to the LIA ELyTLab.

Author contributions

J.d'A., J.-P.R. and C.R. designed experiments; J.d'A. performed experiments and analysed experimental data; J.d'A. and A.S. conceived the particle-based models; A.S. performed simulations and analysed simulation data; C.A. contributed to design of experiments in Supplementary Fig. 1 and provided AprA^{-} cells; F.D. computed the analytical results on bimodal trajectories and helped with the fitting procedure; Y.H. assisted in the data analysis and interpretation; J.d'A. and A.S. wrote the manuscript; F.D., J.-P.R. and C.R. made substantial contributions to the manuscript; all authors discussed and interpreted the data, read and commented on the manuscript; J.-P.R. and C.R. supervised the project.

Additional information

Supplementary information is available in the online version of the paper. Reprints and permissions information is available online at www.nature.com/reprints. Publisher's note: Springer Nature remains neutral with regard to jurisdictional claims in published maps and institutional affiliations. Correspondence and requests for materials should be addressed to J.d'A. or C.R.

Competing financial interests

The authors declare no competing financial interests.

Methods

Cell culture. We used *Dictyostelium discoideum* cells from the strain AX2. The cells were cultured on cell-culture-treated Petri dishes (BD Falcon) in HL5 medium with glucose (Formedium) and kept in a temperature-controlled incubator at 22.5 °C, with a doubling time $\beta^{-1} \sim 9$ h. Before every experiment, the cells were detached from the dish, centrifuged 5 min at 663*g*, harvested and resuspended at the seeding density.

Sample preparation. A reusable mould on Si wafer comprising an array of squares with circular pillars of height ∼150 μm and diameter 320 μm in the centre was fabricated in SU8 photoresist using classical soft-lithography techniques, and its surface was silanized to make it non-adherent. Polydimethylsulfoxide (PDMS, Corning) mixed with curing agent at a 1:10 mass ratio was spin coated on the mould for 1 min at 750 r.p.m. to a target thickness of 70 μm. The squares were cut and peeled off. Usually a thin PDMS membrane obstructed the hole. It was then removed with a surgical blade under the microscope at low magnification.

The square stencil was stuck on the ground of a 3.5 cm wide culture dish and a home-made small plastic well was stuck on it using silicone seal. A droplet of medium was deposited into the well and the sample was placed under vacuum for 15 min to help the medium enter the central hole of the stencil and wet the dish's surface.

The cell suspension was added in the well and the sample was placed in the incubator for 45 min to let the cells sediment and adhere. Then, the plastic well and the stencil were removed with surgical tweezers. Last, the spreading colony was imaged using a slightly defocused bright-field microscope (TE2000, Nikon) at 10× magnification and a wide-field Andor Zyla sCMOS camera. A time-lapse movie was recorded for up to 48 h using MicroManager software with a 20 s time interval, while the temperature was kept constant at 22.5 °C.

For perfusion experiments, we designed a macrofluidic chamber by sealing the culture dish with an adapted cover containing an input and an output tube. The former was linked to a 1 l supply bottle of fresh HL5 medium under controlled overpressure (OB1 controller, Elveflow) while the latter was linked to a disposal bottle. All the system was closed sterilely. We used a flow rate of 100 ml h^{-1} so that the chamber volume of about 10 ml was completely renewed every 6 min. We were thus able to maintain a stable medium renewal over 9 h.

Image processing. The cells' positions were retrieved using home-made ImageJ macros based on the 'Find Maxima' built-in function. Then the individual trajectories were reconstructed with a squared-displacement minimization algorithm (http://site.physics.georgetown.edu/matlab) and the data analysed using home-made Matlab programs.

In particular, the CME was defined as:

$$\mathrm{CME}(\Delta t, t) = \frac{\left\| \mathbf{r}\left(t + \frac{\Delta t}{2}\right) - \mathbf{r}\left(t - \frac{\Delta t}{2}\right) \right\|}{\int_{t'=t-\frac{\Delta t}{2}}^{t+\frac{\Delta t}{2}} \|\mathbf{v}(t')\| \mathrm{d}t'} \tag{3}$$

Simulations. Simulations were carried out by integrating the Langevin equation (2) using a Euler integration scheme with time steps $\Delta t = 10^{-3}$ min. The hard-core repulsion between particles is modelled by a Weeks–Chandler–Andersen potential

$$V(r) = 4[(\sigma/r)^{12} - (\sigma/r)^{6}] + 1 \quad \text{if } r < 2^{1/6}\sigma$$

and 0 otherwise, where $\sigma = 10$ μm is the particle diameter. We define two particles as being in contact when their relative distance $r < \sigma_r = 2^{1/6}\sigma$. In the simulations with CIL, the torque term is turned on only during the contacts, when $r < \sigma_r$. In the simulation including CEL, upon contact cells in low persistence (mode 1) switch to ballistic mode (mode 2), which lasts for an exponentially distributed time with mean duration τ_2.

Data availability. The data that support the plots within this paper and other findings of this study are available from the corresponding authors upon request.